Informatics in Medicine Unlocked 17 (2019) 100176

Contents lists available at ScienceDirect

Informatics in Medicine Unlocked

journal homepage: www.elsevier.com/locate/imu

An efficient 3D color-texture feature and neural network technique for melanoma detection

Firoz Warsi[a], Ruqaiya Khanam[a,*], Suraj Kamya[b], Carmen Paz Suárez-Araujo[c]

[a] Department of ECE, Galgotia University, Greater Noida, India
[b] Department of ECE, IIMT College of Engineering, Greater Noida, India
[c] Instituto Universitario de Ciencias y Tecnologías Cibernéticas, Universidad de Las Palmas de Gran Canaria, Las Palmas de Gran Canaria, Spain

ARTICLE INFO

Keywords:
Melanoma
Color texturefeature
Dermoscopic image
Neural network classifier and skin cancer

ABSTRACT

Malignant melanoma is the deadliest form of skin cancer, but can be more readily treated successfully if detected in its early stages. Due to the increasing incidence of melanoma, research in the field of autonomous melanoma detection has accelerated. In this paper, a new method for feature extraction from dermoscopic images, termed multi-direction 3D color-texture feature (CTF), is proposed, and detection is performed using a back propagation multilayer neural network (NN) classifier. The proposed method is tested on the PH^2 dataset (publicly available) in terms of accuracy, sensitivity, and specificity. The extracted combined CTF is fairly discriminative. When it is input and tested in a neural network classifier that is provided, encouraging results are obtained, i.e. accuracy = 97.5%, sensitivity = 98.1% and specificity = 93.84%. Comparative result analyses with other methods are also discussed, and the results are also improved over benchmarking results for the PH2 dataset.

1. Introduction

One person dies of melanoma every hour [1]. Uncontrolled and abnormal growth of skin cells leads to skin cancer. Unrepaired DNA damage of skin cells cause mutation or triggers genetic defects depending upon which skin cells rapidly multiply and form a malignant tumor. The projected five-year survival rate for early detected melanoma patients is about 99% in the U.S. This falls to 63% when the disease reaches the lymph nodes, and 20% when the disease metastasizes to distant body parts [1].

According to the Skin Care Foundation statistics, one in every three cancers diagnosed is skin cancer. Currently 132,000 melanoma cases occurs globally. Global cases of melanoma are also increasing with ozone layer depletion. A 10% decrease in ozone levels increases the additional cases of melanoma skin cancer by 4500 and non-melanoma skin cancer cases by 300,000 [19,23].

As shown in Fig. 1, it is quite challenging to early classify common nevus, atypical nevus and melanoma [9]. Often the melanomas are black or brown, but they can also be skin-colored, pink, red, purple, blue or white [16,18]. Almost similar steps and sequence are involved in a computer assisted design (CAD) skin disease diagnosis system. These steps involve pre-processing, segmentation, feature extraction and selection, classification and finally testing and result verification as per respective sequence [10,17].

A new approach is proposed in this paper to extract two features i.e. color and texture, as a single feature which is multi-direction 3D (CTF) color texture feature. The lesion component is processed in multiple small windows to evaluate the CTF matrix. This data is further scaled by using gray level spatial dependence matrix as per image intensities. For classification of melanoma and non-melanoma samples, multilayer back propagation neural network classifier is used.

To test and evaluate the system performance the PH^2 data set is used. They are 8-bit RGB color images with a resolution of 768 × 560 pixels. This image database comprises a total of 200 dermoscopic images of melanocytic lesions, containing 80 common nevi, 80 atypical nevi, and 40 melanomas. The PH^2 database contains medical annotations concerning lesion segmentation, clinical and histological diagnosis, along with the assessment of numerous dermoscopic criteria [5,8].

Following this introduction, a brief background is provided for methods to extract feature from dermoscopic images and classifiers for melanoma detection in section 2. The functional block diagram and flow chart of the algorithm along with detailed conceptual logic is described in section 3. Results of the proposed method and comparisons with other novel work in a similar domain are given in section 4, whereas section 5 finally concludes the work and suggests further areas

* Corresponding author.
E-mail addresses: warsifiroz78@gmail.com (F. Warsi), dr.kruqaiya@gmail.com (R. Khanam), kamyasuraj@yahoo.com (S. Kamya), carmenpaz.suarez@ulpgc.es (C.P. Suárez-Araujo).

https://doi.org/10.1016/j.imu.2019.100176
Received 26 November 2018; Received in revised form 22 March 2019; Accepted 28 March 2019
Available online 02 April 2019

Fig. 1. Example of common nevus, atypical nevus and melanoma.

of improvisation.

2. Related work

Feature extraction is a process of vital importance for detection of melanoma in CAD diagnostic systems. Over the last decade a numerous methods to extract various features have been proposed and experiments were done in various color models as well. Although each classifier has its own characteristics and significance but its performance majorly depends upon the uniqueness of the features extracted [13,24].

Texture wavelet, gray-level co-occurrence matrix (GLCM) and shape features are extracted; the performance of various CAD classifiers is compared using these features. A. R. Sadri et al. proposed a technique which completely depends upon fixed wavelet grid network (FWGN) and provides good results i.e. accuracy = 91.82, sensitivity = 92.61, and specificity = 91.00. The construction of FWGN is based on D-optimality orthogonal matching pursuit (DOOMP) which performs image enhancement, segmentation, and classification [2].

C. Barata et al. proposed two methods for detection of melanoma and non-melanoma images using color and texture features. It concludes that both features achieve good results, although color feature outperforms the texture feature. A set of 176 dermoscopic images from Hospital Pedro Hispano, Matosinhos is used to evaluate and test the proposed algorithm. Two methods are addressed, namely local and global. Best results were achieved using global methods when lesion region were divided into two sub-regions which results in a sensitivity 96 and specificity = 80, whereas the results of local system in terms of classification were improved, sensitivity = 100 and specificity = 75 [3].

G. Schaefer et al. extracted the color and texture features from the lesion component of dermoscopic images. A dataset of 564 skin lesion images was obtained from two dermoscopic atlases. For classification, SVM, SMOTE, ensemble and combination of classifiers were proposed. The results of the proposed ensemble classifier system are: accuracy = 93.83, sensitivity 93.76 and specificity = 93.84 [6].

Z. Waheed et al. extracted the color features from HSV domain. The texture feature is extracted using the GLCM method. These features are trained and tested in the SVM classifier. Three-fold cross validation is used to perform classification. Results are obtained using the above feature set and the results are: accuracy = 96, sensitivity = 97 and specificity = 84 [7].

L. Bi et al. used an automatic melanoma detection technique for dermoscopic images via multi-scale lesion-biased representation (MLR) and joint reverse classification (JRC). Skin lesions are represented using closely related histograms. JRC model provides distinctive additional information for melanoma detection. PH^2 public database is used for evaluation and testing of the proposed method. The results show: accuracy = 92, sensitivity = 87.50 and specificity = 93.13 [12].

3. Proposed methadology

Color features provide improved results in comparison to textural features, although the best results are obtained when both are used to classify melanoma [3]. A number of methods are proposed by authors to discretely extract the above two mentioned features [26].

In this paper a new methodology is proposed to extract the two features of color and texture as a single feature, and a multilayer back propagation neural network is used to classify melanoma and non-melanoma images.

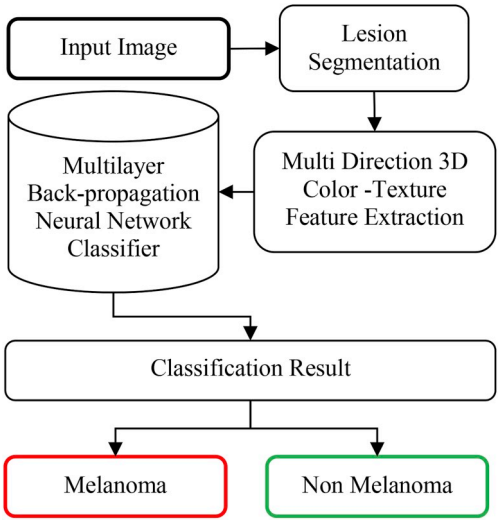

Fig. 2. Functional block diagram of proposed system.

A functional block diagram of the proposed system is provided in Fig. 2.

3.1. Lesion segmentaion

The first and foremost step before extracting any type of information from dermoscopic imagery is to identify the lesion region. The PH^2 database already contains medical annotations which are medical lesion segmentations for all images. An example of melanoma and non-melanoma dermoscopic imagery with its annotated lesion component is respectively shown in Fig. 3 and Fig. 4.

A kernel of 30 × 30 is used to extract the blocks one by one from the complete dermoscopic image. If the extracted blocks have at least 95% pixels from the annotated lesion region, only then are CTF features extracted and further processed from the selected block. To verify that the pixels of the selected block are related to the lesion component or not, a spatial map of the dermoscopic image is used. As per the PH^2 database, each medical image has its respective annotated lesion part. Details of the co-occurrence matrix (CLCM) and the CTF are explained further in the next section.

3.2. Multi direction 3D CTF extraction

Feature plays a significant role in lesion segmentation and classification [11]. Fourteen statistical feature co-occurrence matrices for texture classification were defined by Harlick [20]. Due to the strong correlation between these statistical features, only four out of fourteen are popularly used. The CLCM matrix is based upon GLCM and equations defining it are given below from equations (1)–(4) [14,15].

$$Contrast = \sum_{i,j} |i-j|^2 p(i,j) \tag{1}$$

$$Correlation = \sum_{i,j} \frac{(i-\mu i)(j-\mu j)p(i,j)}{\sigma_i \sigma_j} \tag{2}$$

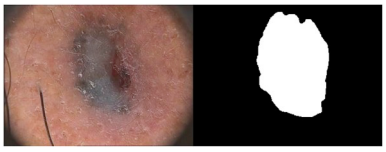

Fig. 3. Melanoma image and its lesion part (PH^2 Dataset).

Fig. 4. Non-Melanoma image and its lesion part (PH^2 Dataset).

$$Energy = \sum_{i,j} p(i,j)^2 \tag{3}$$

$$Homogeneity = \sum_{i,j} \frac{p(i,j)}{1+|i-j|} \tag{4}$$

These equations are useful to compute how many times a pixel with gray level value is correlated to adjacent pixels by value j, and is based on distance d (between pixel of interest and adjacent pixel) and angular spatial relationship theta (Θ = 0, 90, 45 and 135) of an image. The color component of all three planes (R, G, B) are also added while calculating texture feature GLCM; hence the matrix is called CLCM and as both features are calculated in integrity a single feature is used to form the 3D CTF. These three values create a 3D representation of the pixel. The concept of distance (d = 1) and angle (Θ = 0, 90, 45 and 135) between adjacent pixels in a single plane is shown in Fig. 5.

The pixel of interest having intensity 211 is underlined and at distance, d ≈ 1, four pixels are indicated with arrows. The pixel with intensity 205 represents angle 0, pixel with intensity 202 represents angle 45, pixel with intensity 204 represents angle 90, and finally pixel with intensity 203 represents angle 135. Results are calculated with d = 1 and Θ = 0, 90, 45 and 135. Although, in this paper, results shown and discussed are evaluated using distance and angle parameters as d = 1 and Θ = 0, because they outperform the results in comparison to parameters d = 1 and Θ = 90, 45 and 135. The reason for selection of d = 1 is overall computational complexity of the algorithm, which will increase considerably when increasing the kernel size (d > 1).

A sample of 12 × 4 CTF matrices for a 30 × 30 window of the lesion part is demonstrated in Table 1. There is a trade-off between accuracy and computational complexity while selecting window size. Smaller window size will lead to increased computational complexity, whereas the larger window size will lower the accuracy as well as resolution of the feature being extracted. In the table, all four GLCM features, namely contrast, correlation, energy, and homogeneity, are computed respectively as per equations (1) to 4) using factors Θ = 0 and d = 1. The initial three values exhibit d = 0 because the features are computed between pixels of interest in different planes. GLCM and CLCM both use a similar technique to find the features mentioned. The major difference between them is in the method of pixel selection. GLCM selects pixels from only one plane, but CLCM simultaneously selects pixels from all of the three R, G and B planes with variation in Θ, angle, and d, neighborhood distance.

For example, from Fig. 5 suppose that the underlined pixel with intensity 211 is selected, and it is Red plane. The selected pixel can be denoted as (x, y, r) where the third value represents the plane (r – red, g – green and b - blue) [25] and x,y represents the location of the pixel. Now if D = 0 and Θ = 0, then another pixel from the Green plane

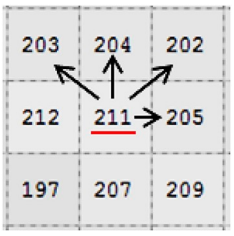

Fig. 5. Adjacent pixels (D = 1 and Θ = 0, 90, 45 and 135).

(x,y,g) is selected to create the first pair of values, known as RG0 as mentioned in Table 1. In case of D = 1 and Θ = 0, the two values will be (x, y, (r/g/b)) and (x, y+1, (r/g/b)) which will create further combinations mentioned in the table, such as RR, GG, BB, RB, RG, GR, GB, BR and BG. Thus in a similar manner a complete 30 × 30 block is extracted from the lesion part of the dermoscopic image. Now using equations (1) to 4), all four properties are computed for 12 sets of different combinations provided in Table 1.

A flow chart for proposed algorithm is shown in Fig. 6. To evaluate the CTF matrix for the complete lesion part, all pixels of interest are selected with a 30 × 30 neighborhood block sequentially from the dermoscopic image, until all of the pixels of the lesion part are processed, and the CTF matrix is also recursively appended for the same. The block selection is done on the basis of the spatial map reference of the lesion part, and CTF is evaluated from the selected block if it contains 95% or more pixels from the lesion part only. In this way, generally a single dermoscopic image is divided into approximately 150–200 blocks of lesion parts. For example, if an image has 200 blocks in the lesion part, then the CTF matrix dimensions will be (200 × 12) 2400 columns and 4 rows of data. This is a large, non-uniform, and computationally complex feature matrix. It is not practically efficient to store and use this large dataset for each image directly with the classifier. The dimension of features extracted in this manner is non-uniform because the lesion part division of each image has a different number of blocks. Hence, to make it computationally efficient and uniform, this large matrix is scaled down from 4 × 2400 to an 8 × 8 matrix, by calculating how often a pixel with particular intensity value i occurs horizontally adjacent to pixel j, or in short, calculating GLCM again for the CTF matrix.

Now the lesion part of each dermoscopic image can be represented by this set of 8 × 8 matrices, irrespective of the numbers of 30 × 30 blocks. This 8 × 8 matrix is converted into a 1 × 64 vector representation before using it in the classifier.

3.3. Multilayer backpropagtion neural network classifier

As per the PH^2 dataset, it consists of a set of 200 dermoscopic images. Out of 200 images, 160 are non-melanoma and 40 are melanoma images. Therefore, the dimension of the input dataset for neural network (NN) is 200 × 64. The target dataset is of 1 × 200 dimension, representing 0 for non-melanoma and 1 for melanoma images.

The NN proposed for classification has 15 hidden layers. Data is divided randomly into three subgroups: training (70%), testing (15%) and validation (15%).

The Scaled conjugate gradient (SCG) back propagation method is used for training the network. This method is based on the conjugate directions [22]. It can train the network as long as the network parameters are derivative. The performance of SCG is already benchmarked against the standard backpropagation. It is based upon well-known optimization techniques for the conjugate gradient method. It yields a speed-up of processing, and also lowers the overall complexity of computation [21].

The proposed algorithm is evaluated in MATLAB. The plot for best validation performance and all confusion matrixes are show in Fig.'s 7 and Fig. 8respectively. As we can analyze from Fig. 7 that test and validation curves vary in a similar manner, so the network is modelled and trained properly.

Basically, the confusion matrix is the simplest measure of the classification model to show how much it is confused while making predictions. The all confusion matrix represents the system performance in terms of accuracy, sensitivity and specificity. It also represents the true positive, true negative, false positive and false negative performances. By this matrix the proposed system's results can be evaluated readily. Results of the proposed system along the comparison with various novel works are given in Table 2.

Table 1
12 × 4 CTF matrix for 30 × 30 block.

Features	1	2	3	4	5	6	7	8	9	10	11	12
D, Θ	0, 0	0, 0	0, 0	1, 0	1, 0	1, 0	1, 0	1, 0	1, 0	1, 0	1, 0	1, 0
Planes	RG0	RB0	BG0	RR	BB	GG	RG	RB	GR	GB	BR	BG
Contrast	1.2675	2.8308	0.5400	0.2142	0.2225	0.2050	1.4058	2.9133	1.3950	0.6125	2.9183	0.6233
Correlation	0.5018	0.4024	0.7300	0.8974	0.8988	0.9097	0.5160	0.4102	0.5152	0.7082	0.4098	0.7172
Energy	0.3982	0.3600	0.3417	0.3484	0.5075	0.3694	0.3242	0.3487	0.3346	0.3407	0.3414	0.3302
Homogeneity	0.8152	0.6305	0.6383	0.7088	0.6513	0.7164	0.6121	0.4769	0.6457	0.5159	0.5124	0.5255

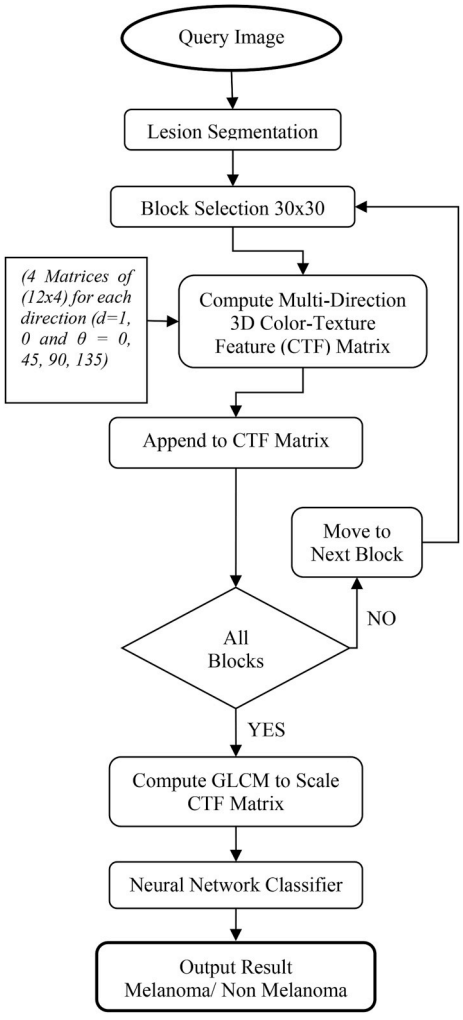

Fig. 6. Flow chart of proposed algorithm.

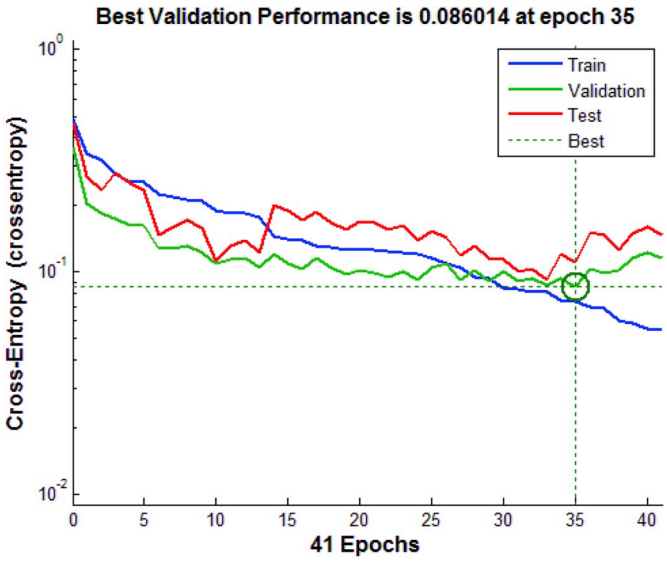

Fig. 7. Best validation performance plot of NN classifier.

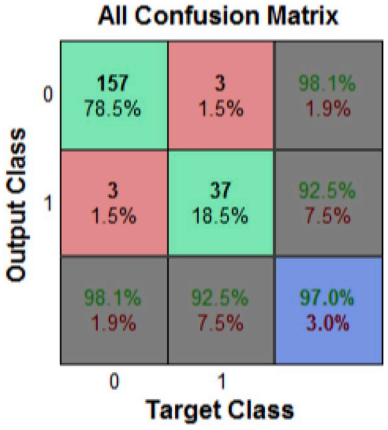

Fig. 8. All confusion matrix of NN classifier.

4. Results and discussion

The results are investigated on the PH^2 dataset of 200 dermoscopic images. The 3D CTF matrix is extracted by combining both texture and color features from all of the three (R, G, B) color planes. Distance and angle parameters are taken as d = 1, Θ = 0. The proposed system is evaluated by accuracy, sensitivity, and specificity in MATLAB, using equations (5)–(7), respectively [4]. True Positive (T_P) provides the number of correctly classified melanoma images; False Positive (F_P) provides the number of incorrectly classified non-melanoma images as melanomas. True Negative (T_N) provides the number of correctly classified non-melanoma images as non-melanomas. False Negative (F_N) provides the number of incorrectly classified non-melanoma

Table 2
Comparative analysis of results.

Sr.	Methods	Accuracy	Sensitivity	Specificity
1	A. R. Sadri [2]	91.82	92.61	91
2	G. Schaefer [6]	93.83	93.76	**93.84**
3	Z. Waheed [7]	96	97	84
4	L. Bi [12]	92	87.5	93.13
5	**Proposed Method**	**97**	**98.1**	92.5

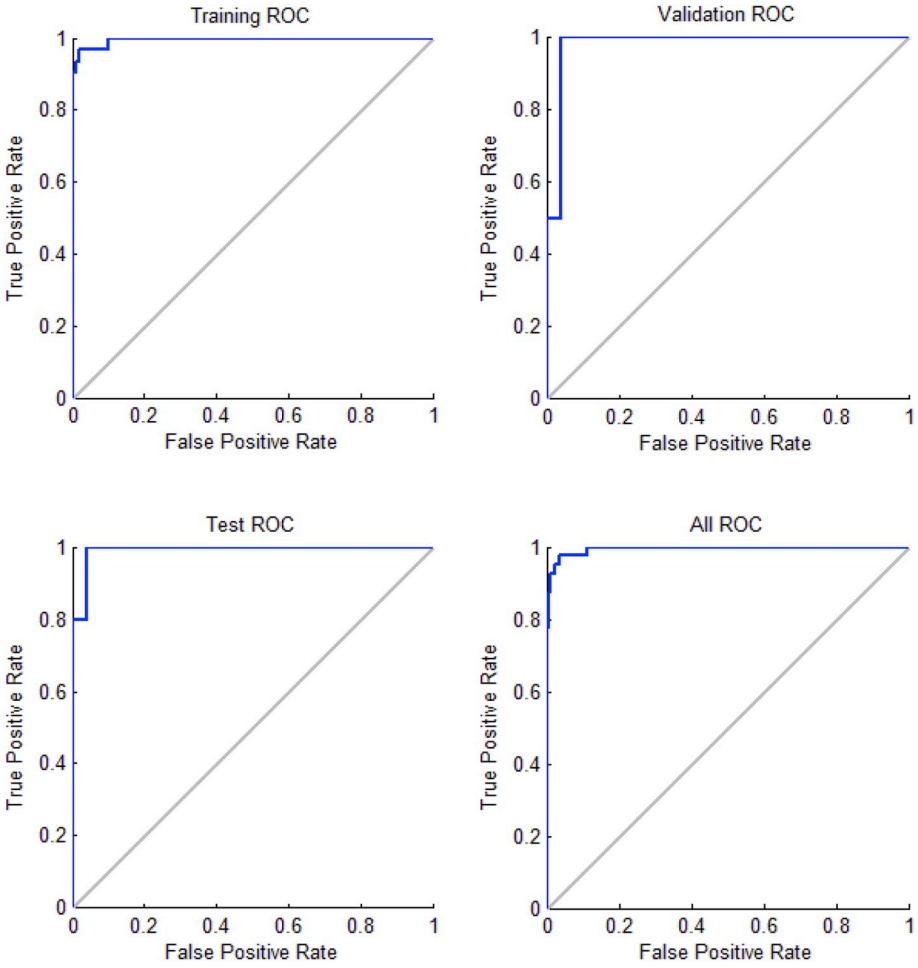

Fig. 9. Receiver operator characteristics (ROC).

images as melanomas. The recognition rate of the system is defined by the accuracy. The Receiver Operating Characteristic (ROC) curve is a graphical representation of the True positive rate (TPR) versus the False Positive Rate (FPR), which is shown in Fig. 9.

The best performance achieved in terms of accuracy is 97%, although a comparative analysis in terms of accuracy, sensitivity and specificity with other novel work is also provided in Table 2.

The results presented are also better than benchmarking results of the PH2 dataset. The benchmarking results are provided on the official website [5] of the PH2 dataset and respected research work [5] is also cited in the reference list.

$$Accuracy = \frac{T_N + T_P}{T_N + F_P + T_P + F_N} \quad (5)$$

$$Sensitivity\ (TPR) = \frac{T_P}{T_P + F_N} \quad (6)$$

$$Specificity\ (TNR) = \frac{T_N}{T_N + F_P} \quad (7)$$

5. Conclusion

A new technique is provided in this paper to compute color and texture features as a single feature which is fairly distinctive, and a back propagation neural network classifier is used to detect melanoma and non-melanoma images. The proposed method provides state-of-the-art results in comparison to various novel methods as shown in Table 2. The results provided are improved over the benchmarking results of the PH2 dataset. In the future, to make system computationally efficient and more accurate, evaluation of this method using various color models, datasets, and classifiers will be further introduced.

Conflicts of interest

No conflict of interest among authors to publishing this article.

Acknowledgement

The authors wish to thank School of Electrical, Electronics and Communication for supporting this work.

Appendix A. Supplementary data

Supplementary data to this article can be found online at https://doi.org/10.1016/j.imu.2019.100176.

References

[1] Cancer facts and figures. American Cancer Society; 2018 Accessed https://www.cancer.org/content/dam/cancer-org/research/cancer-facts-and-statistics/annual-cancer-facts-and-figures/2018/cancer-facts-and-figures-2018.pdf, Accessed date: 3 May 2018.
[2] Sadri AR, et al. WN-based approach to melanoma diagnosis from dermoscopy images. IET Image Process 2017;11(7):475–82.
[3] Barata C, Ruela M, Francisco M, Mendonça T, Marques JS. Two systems for the detection of melanomas in dermoscopy images using texture and color features. IEEE Syst J. 2014;8(3). Sept.
[4] Barata C, Marques JS, Rozeira J. A system for the detection of pigment network in dermoscopy images using directional filters. IEEE Trans Biomed Eng 2012;59(No.

10). October.
[5] Mendonça T, Ferreira PM, Marques J, Marcal ARS, Rozeira J. PH2 - a dermoscopic image database for research and benchmarking. 35th International Conference of the IEEE Engineering in Medicine and Biology Society, July 3-7, Osaka, Japan. 2013https://www.fc.up.pt/addi/ph2%20database.html.
[6] Schaefer G, Krawczyk B, Emre Celebi M, Iyatomi H. Melanoma classification using dermoscopy imaging and ensemble learning. Second IAPR Asian Conference on Pattern Recognition. 2013.
[7] Waheed Z, Waheed A, Zafar M, Riaz F. An efficient machine learning approach for the detection of melanoma using dermoscopic images. International Conference on Communication, Computing and Digital Systems (C-CODE), 8-9 March. 2017.
[8] Gu Yanyang, Zhou Jun, Qian Bin. Melanoma detection based on mahalanobis distance learning and constrained graph regularized nonnegative matrix factorization. IEEE Winter Conference onApplications of Computer Vision (WACV), 24-31 March. 2017.
[9] Satheesha TY, Satyanarayana D, Prasad MN Giri, D Dhruve K. Melanoma is skin deep: a 3D reconstruction technique for computerized dermoscopic skin lesion classification. IEEE J. Transl. Eng. Health. Med 2017(5). Jan.
[10] Jafari MH, Nasr-Esfahani E, Karimi N, Soroush-mehr SM, Samavi S, Najarian K. Extraction of skin lesions from non-dermoscopic images using deep learning. 2016.
[11] Hameed N, Ruskin A, Hassan KA. A comprehensive survey on image-based computer aided diagnosis systems for skin cancer. 10th International Conference on Software, Knowledge, Information Management and Applications (SKIMA). 2016.
[12] Bi L, Kim J, Ahn E, Feng D, Fulham M. Automatic melanoma detection via multi-scale lesion-based representation and joint reverse classification. 13th International Symposium on Biomedical Imaging (ISBI). 2016. April.
[13] Julesz B. A theory of preattentive texture discrimination based on first-order statistics of textons. Biol Cybern 1981;41:131–8.
[14] Benco M, Hudec R, Kamencay P, Zachariasova M, Matuska S. An advanced approach to extraction of color texture features based on GLCM. Int J Adv Robot Syst 2014:1–8.
[15] Nailon WH, Mao Y. Texture analysis methods for medical image characterisation. Biomedical Imaging IntechOpen; 2010. https://doi.org/10.5772/8912. March 1st.
[16] Maglogiannis I, Doukas CN. Overview of advanced computer vision systems for skin lesions characterization. IEEE Trans Inf Technol Biomed September 2009;13(5):721–33.
[17] Iyatomi H, Oka H, Celebi ME, Hashimoto M, Hagiwara M, Tanaka M, Ogawa K. An improved Internet-based melanoma screening system with dermatologist-like tumor area extraction algorithm. Comput Med Imag Graph 2008;32(7):566–79.
[18] Stolz W, Riemann A, Cognetta AB. ABCD rule of dermatoscopy: a new practical method for early recognition of malignant melanoma. Eur J Dermatol 1994;4(7):521–7.
[19] Baldwin L, Dunn J. Global controversies and advances in skin cancer. Asian Pac. J. Cancer Prev. APJCP 2013;14:2155–7.
[20] Haralick RM, Shanmugam K. Dinstein Its'Hak textural features for image classification, systems, man and cybernetics SMC IEEE Trans. 1973;3(6):610–21.
[21] Moller. Neural Network 1993;6:525–33.
[22] Aich A, Dutta A, Chakraborty A. A scaled conjugate gradient backpropagation algorithm for keyword extraction. In: Bhateja V, Nguyen B, Nguyen N, Satapathy S, Le DN, editors. Information Systems Design and Intelligent Applications. Advances in Intelligent Systems and Computing, vol. 672. Singapore: Springer; 2018.
[23] Ultraviolet radiation and the INTERSUN programme, WHO. https://www.who.int/uv/faq/skincancer/en/index1.html.
[24] Blum A, Rassner G, Garbe C. Modified ABC-point list of dermoscopy:A simplified and highly accurate dermoscopic algorithm for the diagnosis of cutaneous melanocytic lesions. J Am Acad Dermatol 2003;48(5):672–8. May.
[25] Glaister J, Wong A, Clausi DA. Segmentation of skin lesions from digital images using joint statistical texture distinctiveness. IEEE Trans Biomed Eng Apr 2014;61(4):1220–30.
[26] Abuzaghleh O, Faezipour M, Barkana BD. A comparison of feature sets for an automated skin lesion analysis system for melanoma early detection and prevention. IEEE Long Island Systems, Applications and Technology Conference. 2015.